New Journal of Physics
The open–access journal for physics

Structure–function relationship in complex brain networks expressed by hierarchical synchronization

Changsong Zhou[1,3], Lucia Zemanová[1], Gorka Zamora-López[1], Claus C Hilgetag[2] and Jürgen Kurths[1]

[1] Institute of Physics, University of Potsdam, PF 601553, 14415 Potsdam, Germany

[2] Jacobs University Bremen, Campus Ring 6, Rm 116, D-28759 Bremen, Germany

E-mail: cszhou@agnld.uni-potsdam.de

New Journal of Physics **9** (2007) 178
Received 31 January 2007
Published 28 June 2007
Online at http://www.njp.org/
doi:10.1088/1367-2630/9/6/178

Abstract. The brain is one of the most complex systems in nature, with a structured complex connectivity. Recently, large-scale corticocortical connectivities, both structural and functional, have received a great deal of research attention, especially using the approach of complex network analysis. Understanding the relationship between structural and functional connectivity is of crucial importance in neuroscience. Here we try to illuminate this relationship by studying synchronization dynamics in a realistic anatomical network of cat cortical connectivity. We model the nodes (cortical areas) by a neural mass model (population model) or by a subnetwork of interacting excitable neurons (multilevel model). We show that if the dynamics is characterized by well-defined oscillations (neural mass model and subnetworks with strong couplings), the synchronization patterns are mainly determined by the node intensity (total input strengths of a node) and the detailed network topology is rather irrelevant. On the other hand, the multilevel model with weak couplings displays more irregular, biologically plausible dynamics, and the synchronization patterns reveal a hierarchical cluster organization in the network structure. The relationship between structural and functional connectivity at different levels of synchronization is explored. Thus, the study of synchronization in a multilevel complex network model of cortex can provide insights into the relationship between network topology and functional organization of complex brain networks.

[3] Author to whom any correspondence should be addressed.

PII: S1367-2630(07)42936-6

Contents

1. Introduction

Synchronization of distributed brain activity has been proposed as an important mechanism for neural information processing [1]. The experimentally observed brain activity, characterized by synchronization phenomena over a wide range of spatial and temporal scales, reflects a hierarchical organization of the dynamics [2]. Structurally, the cortical networks display a hierarchy of complex connectivity [3]: the microscopic level of interacting neurons, the mesoscopic level of minicolumns and local neural circuits, and the macroscopic level of nerve fibre projections between brain areas [4]. While details at the first two levels are still largely missing, extensive information has been collected about the latter level in the brain of animals, such as cats [4] and macaque monkeys [5]. The analysis of the anatomical connectivity of the mammalian cortex (see a recent review [6]) has shown that large-scale cortical networks display typical features of small-world networks, e.g. high clustering and short pathlength. This allows the system to perform both specialized and integrated processes. Additionally, the robustness of cortical networks against node lesion exhibits properties similar to those of scale-free networks [7].

In parallel, during recent years, investigation of brain activity has also put significant emphasis on the large-scale *functional interactions* between brain areas. Modern brain imaging techniques, e.g. functional magnetic resonance imaging (fMRI), allow to follow, dynamically and noninvasively, various markers of brain activity. Numerous linear or nonlinear time series analysis methods have been applied to study the functional connectivity between brain areas, and the complex network analysis approach has been employed to explore the structural organization of large-scale functional brain networks [8]–[11]. Similar to anatomical networks, the functional networks also display features of small-world and scale-free networks [8]. The functional connectivity of brain networks based on fMRI is characterized by its dependence on frequency; it is denser and stronger at slow timescales [11].

An important problem in cognitive neuroscience is the understanding of the relationship between anatomical and functional connectivity. Due to the invasive nature of neuroanatomical techniques (mainly by tracer injection), the most complete data about anatomical connectivity are available only for animal brains, while the topological properties of the human connectome

remain largely unclear [3]. For this reason, a direct comparison of the large-scale functional networks from human fMRI with anatomical connectivity does not seem feasible within the foreseeable future.

To better understand the principles underlying the dynamics of cortical systems, computational neuroscience has for a long time focused on the dynamics of various models of neuronal networks. The dynamical regimes, such as asynchronous on-going activity with balancing between excitation and inhibition [12], have been investigated within globally or sparsely and randomly connected architectures [12, 13]. Systematic exploration of the impact of connection topology on the dynamical organization in neuronal networks (which is barely beginning) will be an important direction in neuroscience. Recently, the extraction of connectivity patterns between different types of neurons at the level of cellular circuits has been described [14]. Based on such data an ambitious project, the Blue Brain Project [15], aims to build a detailed and large-scale computer model of a mammalian brain. So far, such models could be built for local neuronal circuits using realistic morphological properties of neurons and neuronal connectivity. However, this 'bottom-up' approach faces a huge gap of information regarding the detailed neuronal connectivity between distant cortical regions. Thus, the relationship between anatomical and functional connectivity, especially over a range of scales, remains one of the major challenges in neuroscience [1].

We focus on the systems level of the connectivity formed by long-range projections among cortical areas as described in section 2. Our main goal is to investigate the synchronization behaviour of a realistic network of corticocortical connections and study the relationship between the global dynamical organization and the network connectivity at the systems level. We simulate the dynamics of the nodes (cortical areas) in the networks with various models. The first choice (intuitively) is to use a neural mass model (low dimensional dynamical model describing the mean activity of neuronal populations [16, 17]). The results using this *population model* are presented in section 3. We show that such a model, displaying dynamics with a well-defined single timescale (alpha waves), generates dynamical patterns largely determined by the total input strength (intensity) of nodes, but not by the detailed network topology. A more realistic choice, presented in section 4, is to implement a 'bottom-up' approach representing each network node (cortical area) by a subnetwork of interacting excitable neurons. Different from the 'Blue Brain Project', we use a recurrent network with typical small-world topology which accounts for the basic features of realistic neuronal connectivity at the cellular level [18]. The simulated system, *a network of networks*, represents a *multilevel model* and displays biologically plausible dynamical regimes. Here the dynamics shows a hierarchical organization revealing different levels of modular organization in the anatomical connectivity of the corticocortical networks.

A detailed description of the multilevel model and analysis of the major dynamical regimes are given in [19]. In [20], we briefly account for the main results of the multilevel model in its biologically realistic regime. Here, we present an extensive description of our modelling schemes, including the results of population model and a more detailed analysis of the multilevel model, and also a comparison between both types of modelling.

2. Corticocortical network of cat

In this paper, we use the cat corticocortical network as an example for large-scale anatomical connectivity. The cerebral cortex of a cat can be parcellated into 53 areas, linked by about

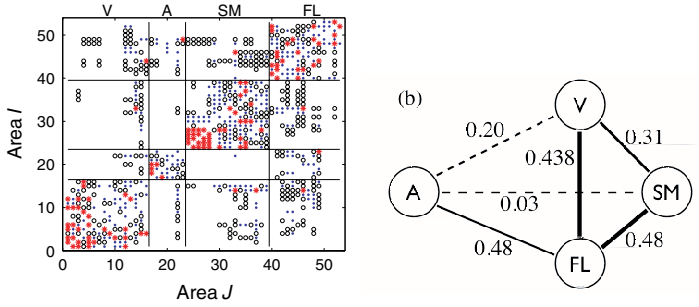

Figure 1. (a) Connection matrix M^{A} of the cortical network of the cat brain. The different symbols represent different connection weights: 1 (○ sparse), 2 (● intermediate) and 3 (∗ dense). The organization of the system into four topological communities (functional sub-systems, V, A, SM, FL) is indicated by the solid lines. (b) The density of connections between the four communities.

830 fibres of different densities [4] into a weighted complex network as shown in figure 1(a). This network displays typical small-world properties, i.e. short average pathlength and high clustering coefficient, indicating an optimal organization for effective inter-area communication and for achieving high functional complexity [21, 22]. The degree of the nodes is heterogeneous, several nodes have only 2–3 links while others have up to 35 connections. Due to the small size of the network, it is difficult to claim that degree follows a scale-free distribution [23]. Nevertheless, the distribution is very close to that of networks of the same size and density generated by scale-free models [23].

Different from random network models, the cortical network of the cat exhibits a hierarchically clustered organization [22, 24]. There exist a small number of topological clusters that broadly agree with four functional cortical sub-divisions: visual cortex (V, 16 areas), auditory (A, 7 areas), somato-motor (SM, 16 areas) and fronto-limbic (FL, 14 areas). To distinguish from the dynamical clusters, we will refer to the topological clusters as *communities* [25]. Figure 1(b) shows that community A is sparsely connected while communities V, SM and FL are densely connected among each other.

3. Neural mass model (population model)

In this section, we study the dynamics of the cat cortical network representing each cortical area by a neural mass model. Such a model describes the activities of a population of cortical neurons.

The mean activity of a population of neurons in the brain often exhibits rhythmic oscillations with well-defined frequency bands, as seen in EEG measurements [26]. Such oscillations can be reproduced by realistic macroscopic models of EEG dynamics proposed since the early 1970s [16, 17, 27]. We use the neural mass model and parameters presented in [17]. A population of neurons contains two subpopulations: subset 1 consists of pyramidal cells receiving excitatory or inhibitory feedback from subset 2. Subset 2 is composed of local interneurons receiving excitatory inputs. This model describes the evolution of the macroscopic variables, i.e. average post-synaptic membrane potentials v^{p} for pyramidal cells, and v^{e}, v^{i} for the excitatory and inhibitory

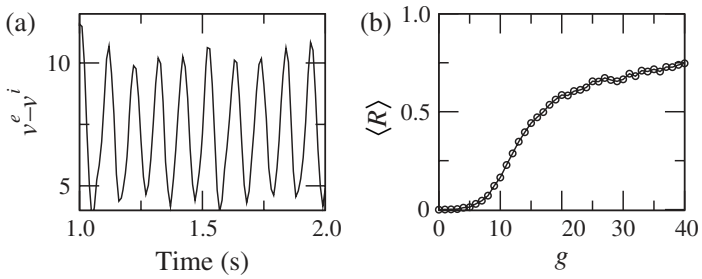

Figure 2. (a) Typical activity $V = v^{\mathrm{e}} - v^{\mathrm{i}}$ of the uncoupled neural mass model. (b) The average correlation coefficient $\langle R \rangle = \frac{1}{N(N-1)} \sum_{I \neq J} R_{IJ}$ ($N = 53$) versus the coupling strength g in equation (3).

interneurons, respectively. A static nonlinear sigmoid function $f(v) = 2e_0/(1 + \mathrm{e}^{r(v_0 - v)})$ converts the average membrane potential into an average pulse density of action potentials. Here v_0 is the post-synaptic potential corresponding to a firing rate of e_0, and r is the steepness of the activation. The external input from other groups of neurons and noise are fed into the population of interneurons. The dynamical equations for $I = 1, \ldots, N$ multiple coupled populations read

$$\ddot{v}_I^{\mathrm{p}} = Aaf(v_I^{\mathrm{e}} - v_I^{\mathrm{i}}) - 2a\dot{v}_I^{\mathrm{p}} - a^2 v_I^{\mathrm{p}}, \tag{1}$$

$$\ddot{v}_I^{\mathrm{i}} = BbC_4 f(C_3 v_I^{\mathrm{p}}) - 2b\dot{v}_I^{\mathrm{i}} - b^2 v_I^{\mathrm{i}}, \tag{2}$$

$$\ddot{v}_I^{\mathrm{e}} = Aa\left[C_2 f(C_1 v_I^{\mathrm{p}}) + p_I(t) + \frac{g}{\langle S \rangle} \sum_J^N M_{IJ}^{\mathrm{A}} f(v_J^{\mathrm{e}} - v_J^{\mathrm{i}})\right] - 2a\dot{v}_I^{\mathrm{e}} - a^2 v_I^{\mathrm{e}}, \tag{3}$$

where v_I^{p}, v_I^{i} and v_I^{e} are the post-synaptic membrane potentials of the area I. The parameters A and B represent the average synaptic gains, $1/a$ and $1/b$ the average dendritic-membrane time constants. C_1 and C_2, C_3 and C_4 are the average number of synaptic contacts, for the excitatory and inhibitory synapses, respectively. A more detailed interpretation and the standard parameter values of this model can be found in [17]. To model the cat cortical network by such macroscopic neural mass oscillators, we take the anatomical connectivity in figure 1(a) as the coupling matrix M_{IJ}^{A} in equation (3). We normalize coupling strength g by the mean intensity $\langle S \rangle$ where the intensity $S_I = \sum_J^N M_{IJ}^{\mathrm{A}}$ is the total input weight to node I.

As in [17], in our simulations we take $p_I(t) = p_0 + \xi_I(t)$ where $\xi_I(t)$ is Gaussian white noise with standard deviation $D = 2$. The main results do not show a sensitive dependence on D. We fix $p_0 = 180$ so that the system is in the periodic regime corresponding to alpha waves. A typical time series of the output, the average potential $V_I = v_I^{\mathrm{e}} - v_I^{\mathrm{i}}$, is shown in figure 2(a).

Synchronization between the areas is measured by the linear correlation coefficient R_{IJ} between the outputs V_I and V_J. Other measures, such as phase synchronization, would provide very similar information about the intercorrelation between the areas. The average correlation $\langle R \rangle$ among all pairs of areas is shown in figure 2(b) as a function of the coupling strength g. The results indicate that no clear correlation is established for weak coupling $g < 5$, while some nontrivial correlation seems to be expressed for larger coupling values. The dynamical pattern

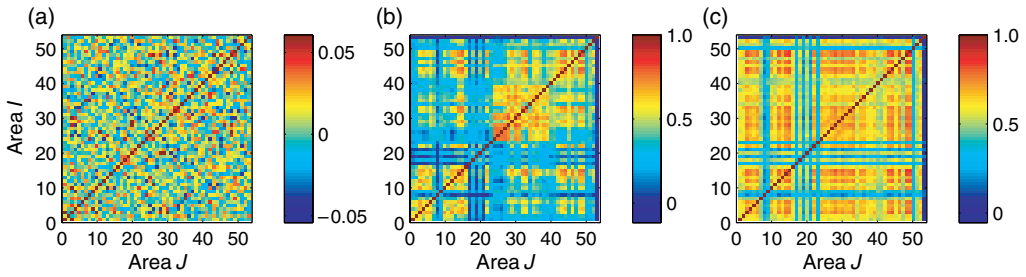

Figure 3. Correlation matrices R_{IJ} of population model of the cat cortical network at weak coupling $g = 2$ (a) and strong coupling $g = 15$ (b). (c) R_{IJ} of a randomized network with $g = 15$. Note the different grey-scales in the colourbars.

is not structured at very weak coupling, but at stronger couplings ($g \geqslant 5$), the system forms a large synchronized cluster including most of the areas from V, SM and FL, while the auditory system A remains relatively independent (figure 3). This is consistent with the inter-community connectivity shown in figure 1(b).

According to our previous analysis of general random networks [28] of coupled oscillators (x_I), with a strong enough coupling the whole network achieves a high level of synchronization expressed as a collective oscillation in the mean activity $X = (1/N)\sum_I^N x_I$. Although the cat cortical network exhibits an organization of communities, it also possesses many random-like connections between the communities. A mean field approximation might still provide a meaningful understanding of the dynamical organization in the strong coupling regime. With this approximation, the average input that a node I receives from its k_I direct neighbours, $(1/k_I)\sum_J^N M_{IJ}^{\mathrm{A}} f(V_J)$, can be replaced by the mean activity $f(X)$, where $X = (1/N)\sum_J^N V_J$. The coupling term in equation (3) can be written as

$$\frac{g}{\langle S\rangle}\sum_J^N M_{IJ}^{\mathrm{A}} f(v_J^{\mathrm{e}} - v_J^{\mathrm{i}}) \approx \frac{gS_I}{\langle S\rangle} f(X). \tag{4}$$

In this first-order approximation, the nonlinearity of the sigmoid function $f(v)$ is also neglected. It means that nodes with large intensities S are more strongly coupled to the global mean field X. These nodes synchronizing commonly with X form an effective cluster, while the nodes with small intensities S are not significantly influenced by the activity of other nodes and preserve their own, rather independent, dynamics.

The above analysis has been largely confirmed by our simulations. We calculate the correlation coefficient R_X between the activity V_I of an area and the global mean field $X = (1/N)\sum_I^N V_I$. In figure 4, R_X is averaged for nodes with the same values of intensity S and plotted for various coupling strengths. It is roughly an increasing function of S. We have carried out simulations on randomized cat cortical networks, maintaining both the input degree k_I and intensity S_I of all the nodes [29]. In this case results of R_X shows again monotonous increase with the intensity S (figure 4, solid line). The fluctuation of R_X of the original cortical network is mainly due to the clustered organization at various levels (figure 4, dashed line). For a more detailed comparison, we also show a typical correlation pattern of these randomized networks, figure 3(c). As we see, the major dynamical organization is very similar for both the cat network and the randomized network. This similarity shows that dynamics using a neural

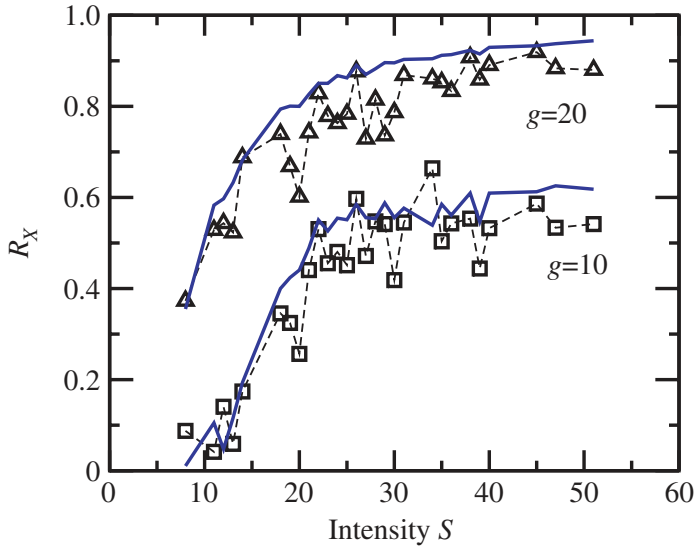

Figure 4. Correlation R_X between the activity of an area V_I and the global mean field X, as a function of the intensity S (averaged over nodes with the same intensity S) at various coupling strength g. Dashed line represents the original cat cortical network, and solid line the randomized matrix.

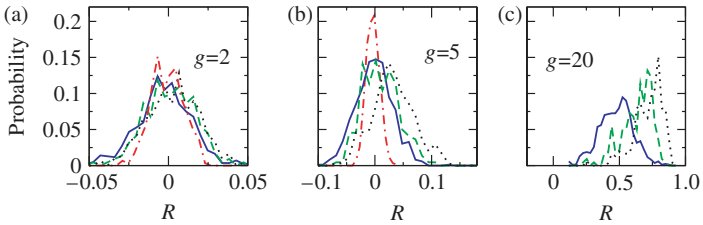

Figure 5. Distribution of the correlation R for P0 (solid line), P1 (dashed line) and P2 (dotted line) pairs at various values of the coupling strength g, (a) $g = 2$, (b) $g = 5$ and (c) $g = 20$. The dash-dotted lines in (a) and (b) indicate the distribution between uncoupled areas ($g = 0$) and the different shapes of the distributions in (a) and (b) are due to different bin sizes.

mass oscillator depend only little on the detailed network topology, but largely on the input intensity of the nodes. A direct and strong relationship between the pair-wise coupling M^{A}_{IJ} and the strength of synchronization R_{IJ} is not observed. To demonstrate this, we distinguish three cases for any pair of nodes in the network: reciprocal projections (P2), uni-directional couplings (P1) and non-connection (P0). We compute the distribution of the correlation R_{IJ} for these cases separately. As seen in figure 5, when the coupling is weak (e.g. $g = 2$), the distributions for P0, P1 and P2 pairs coincide and display a Gaussian shape around zero. Compared to the distribution obtained by computing the correlation for uncoupled nodes ($g = 0$) (figure 5, dash-dotted lines), we can see that most of the correlations are insignificant. At a stronger coupling (e.g. $g = 5$), the P2 pairs have slightly stronger correlation than P1, however, the distributions still significantly overlap, as it is similar for strong couplings.

In summary, our results using generic oscillators (in this case, neural mass oscillators) show the dependence of the dynamics on the single node characteristics, but the network topology is not very relevant. Such a feature comes from the well expressed, single-scale oscillation generated by the model. When coupled with strong enough strength, such sustained oscillations represent the fact that the neural activity propagates continuously from a node to its neighbours and next neighbours in the network, and produces a collective oscillation of the whole system. In reality, continuous and large-scale spreading of neural activity in a strongly synchronized manner occurs only in pathological situations, such as epileptic seizure [13]; in a normal brain, the spontaneous EEG contains a broad range of timescales [27] which is not accounted for by this model. Thus, such a simplified model of EEG generation, when assuming a periodic oscillation, seems to be not suitable to reflect the relationship between the intricate structural and functional connectivities of cortical networks, especially in a normal rest state with a background spontaneous activity. Note, however, coupling several neural mass oscillators in some particular ways representing forward, backward and lateral processes has been proposed to model event-related responses in the brain [30]. Estimation of the coupling parameters of such models using empirical data can be used to assess causal (effective) connectivity between brain areas [31].

Another option is to use models of coupled excitable elements with structured connectivity, as we will try in the next section.

4. Subnetworks of interacting neurons (multilevel model)

4.1. Description of the model

Now we model each cortical area with a subnetwork of N_a interacting neurons. We consider local neurons to be coupled with a small-world topology (SWN [32]) to reproduce basic biological features: neurons are mainly connected to their spatial neighbours, but a few long-range projections are also present [19]. The SWN topology has been shown to improve synchronization of interacting neurons [33]–[35] and to maintain persistent activity [36]. In particular, a regular array of N_a neurons with a mean degree k_a is rewired with a probability p. Our model also includes other realistic, experimentally observed features: 25% of the N_a neurons are inhibitory and only a small number of neurons (about 5%) in one area receive excitatory synapses from other areas [37]. We assume that cortical areas communicate with each other via their mean field activity. Individual neurons are described by the FitzHugh–Nagumo (FHN) excitable model [38] with non-identical excitability. A weak Gaussian white noise (with strength $D = 0.03$) is added to each neuron so that isolated units exhibit sparse, Poisson-like irregular spiking patterns, as in realistic neurons.

Thus our multilevel model of the neural network of a cat cortex consists of a *network of networks* of noisy neurons. The dynamics of each neuron i in area I reads:

$$\epsilon \dot{x}_{I,i} = f(x_{I,i}) + \frac{g}{k_a} \sum_{j}^{N_a} M_I^{\mathrm{L}}(i,j)(x_{I,j} - x_{I,i}) + \frac{g}{\langle w \rangle} \sum_{J}^{N} M_{IJ}^{\mathrm{A}} L_{IJ}(i)(V_J - x_{I,i}), \tag{5}$$

$$\dot{y}_{I,i} = x_{I,i} + a_{I,i} + D\xi_{I,i}(t), \tag{6}$$

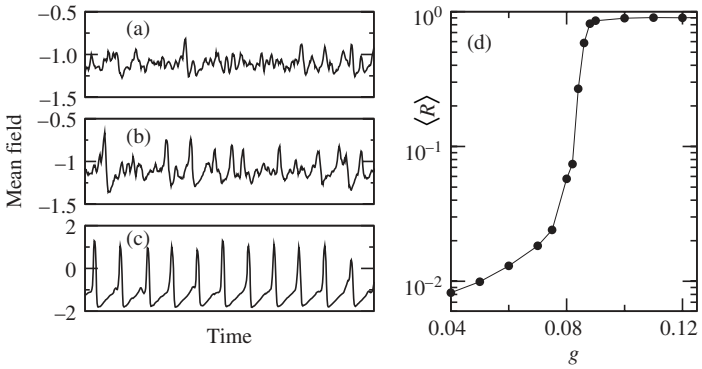

Figure 6. Typical mean activity V_I of one area at various coupling strengths (a) $g = 0.07$, (b) $g = 0.082$, (c) $g = 0.09$. The average correlation coefficient $\langle R\rangle = \frac{1}{N(N-1)}\sum_{I\neq J} R_{IJ}$ $(N = 53)$ versus g.

where

$$f(x_{I,i}) = x_{I,i} - \frac{x_{I,i}^3}{3} - y_{I,i}. \tag{7}$$

Here the matrix M^{A} represents the corticocortical connections in the cat network as in figure 1(a). M_I^{L} denotes the local SWN of the Ith area ($M_I^{\mathrm{L}}(i, j)$: $i, j = 1, \ldots, N_{\mathrm{a}}$). If neuron j is inhibitory then $M_I^{\mathrm{L}}(i, j) = -1$ for all of its connected neighbours. The label $L_{IJ}(i) = 1$ if the neuron i is among the 5% within the area I receiving the mean field signal $V_J = (1/N)\sum_l^{N_{\mathrm{a}}} x_{J,l}$ from the area J, otherwise, $L_{IJ}(i) = 0$. The diffusive coupling which represents the electrical interaction between the neurons, is not the most typical case in the mammalian cortex, but is mainly considered for the simplicity of simulation at this stage. The average coupling strength between any pair of neurons g is the control parameter in our simulations. Note that we assume g to be equal for couplings within and between subnetworks. We normalize it by the mean degree k_{a} of the SWNs within the areas and by the average weight $\langle w\rangle$ of inter-area connections. The system is simulated with $N_{\mathrm{a}} = 200$, $k_{\mathrm{a}} = 12$ and $p = 0.3$ for the subnetworks. Our focus is to study the synchronization behaviour at the systems level, i.e. the correlation between the mean activity V_I of the subnetworks and its relationship to the underlying cortical topology (figure 1(a)). The synchronization behaviour between cortical areas, demonstrated in the following sections, does not depend critically on the parameters of the subnetworks. However, detailed dynamics *within* the subnetwork does depend on them [33]–[36].

4.2. General dynamics

The coupling strength g controls the mutual excitation among the neurons. At small g (e.g. $g = 0.07$), a neuron is not often excited by the noise-induced spiking of its connected neighbours, so the synchronization within and between the subnetworks is weak. This is shown by the small fluctuations of the mean activity V_I of each area (figure 6(a)) and a small average correlation coefficient $\langle R\rangle$ between them (figure 6(d)). Weak synchronization in the subnetwork of an area is manifested by a few peaks in V_I (figure 6(a)). Increasing g, the synchronization becomes stronger

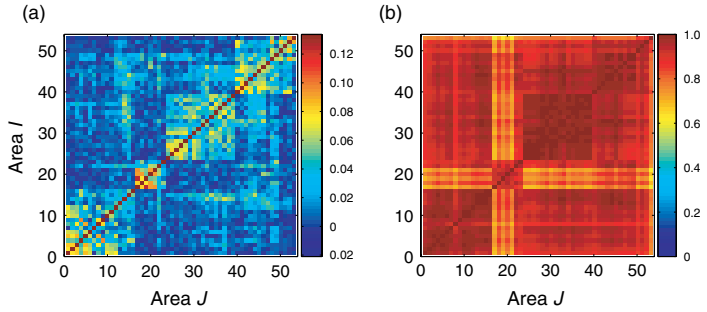

Figure 7. Correlation matrices R_{IJ} at weak coupling $g = 0.07$ (a) and strong coupling $g = 0.12$ (b).

with more frequent and larger peaks in V_I (figure 6(b)) and at large enough g, the neurons are mutually excited achieving both strongly synchronized and regular spiking behaviour (figure 6(c)). In this case $\langle R \rangle$ approaches to 1 (figure 6(d)), indicating an almost global synchronization of the network.

The correlation matrices R_{IJ} for different g are shown in figure 7. At strong coupling (figure 7(a)), the pattern of correlations is very similar to that of the neural mass model since both models display well-defined oscillations. However, the weak coupling dynamics in this multilevel model has a nontrivial organization and an intriguing relationship to the underlying network topology, see figure 7(a). The distribution of R among all pairs of areas displays a Gaussian peak around zero, but with a long-tail to large values (figure 8(a), solid line). Although the correlations are relatively small, we find that the large values are significant when compared to the distribution of R of surrogate data by random shuffling of the time series V_I (figure 8(a), dash-dotted line). The weak coupling regime is biologically more realistic, since here the neurons only have a low frequency of irregular spiking and irregular mean activities (figure 6(a)), similar to those observed experimentally (e.g. EEG data [27]). The propagation of a signal between connected areas is mediated by synchronized activities (peaks in V) and a temporal correlation is most likely established when the receivers produce similar synchronized activities by this input, or when two areas are excited by correlated signals from common neighbours. Due to the weak coupling and the existence of subnetworks, such a synchronized response does not always occur and a local signal (excitation) does not propagate through the whole network. As a result, the correlation patterns are closely related to the network topology, although the values are relatively small due to infrequent signal propagation. With strong couplings, the signal can propagate through the whole network, corresponding to pathological situations, such as epileptic seizure [13].

Let us now characterize the dynamical organization and its relationship with the network topology. Based on the argument of signal propagation, we expect the correlations for the P2, P1 and P0 areas to be significantly different. Indeed, the distributions of R for these three cases display well-separated peaks in the weak coupling regime (figure 8(a)). Especially, all the P2 pairs have significant correlations compared to the surrogate data. At strong coupling (e.g. $g > 0.09$), where the excitation propagates through the whole network, the distribution is very similar to the neural mass model in figure 5(c), and the separation is no longer pronounced (figure 8(b)).

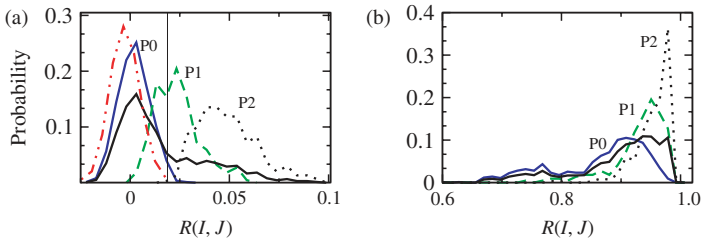

Figure 8. Distribution of the correlation R ($g = 0.07$) for all nodes (solid line), P2 (dotted line), P1 (dashed line) and P0 (blue solid line). The dash-dotted line denotes the results for the surrogate data.

4.3. Functional connectivity

In the following section, we want to study more closely the relationship between the anatomical topology and functional connectivity. We extract *functional networks* M^{F} from the dynamics of the multilevel model by applying a threshold R_{th} to the correlation matrix R_{IJ} so that a pair of areas is considered to be functionally connected if the correlation between them is larger than the threshold [9]–[11]:

$$M^{\mathrm{F}}_{IJ} = \begin{cases} 1 & \text{if } R_{IJ} \leqslant R_{\mathrm{th}} \\ 0 & \text{otherwise} \end{cases}$$

We compare these functional networks M^{F} at different R_{th} to the topological features of the anatomical network M^{A} and examine how the various levels of synchronization reveal different scales in the topology. We focus on the biologically meaningful weak coupling regime and take $g = 0.07$ as the typical case.

In order to characterize the functional relevance of *anatomical* features, we use several graph theoretical measures. Our results in figure 8(a) show dependence of the correlation on the link reciprocity. Furthermore, it is expected to depend on the connection weights. To account for both the topology and strength of connections, we define the *reciprocal weight*, w_{IJ}, as the normalized sum of the links between I and J:

$$w_{IJ} \equiv (M^{\mathrm{A}}_{IJ} + M^{\mathrm{A}}_{JI})/6,$$

(where 6 is the maximal bidirectional weight). In figure 9(a) the pair-wise w_{IJ} are shown for the anatomical connectivity matrix M^{A}.

However, pair-wise connection weight alone does not completely explain the strength of correlation between two areas, the common environment of areas might also play an important role. The *matching index* between two nodes, $MI(i, j)$, is the number of their common neighbours, thus, it can be regarded as a measure for pair-wise *functional similarity* [39]. It is quantified as:

$$MI(i, j) = \sum_{l=1}^{N} A_{il} A_{jl}$$

where A_{ij} is the adjacency matrix of a network. A proper normalization is obtained by dividing each element of the MI matrix by $(k_i + k_j - MI(i, j))$ that is the total number of distinct nodes to

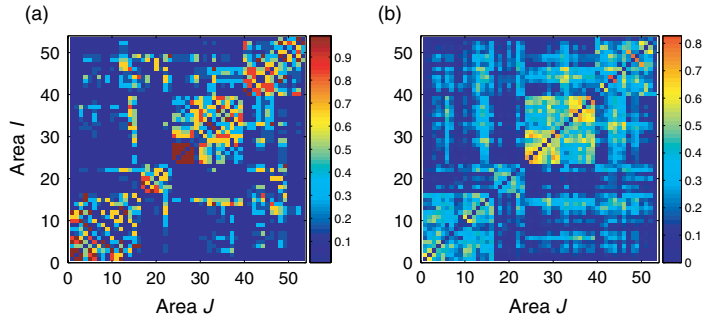

Figure 9. Pair-wise properties of the anatomical network M^{A}: (a) reciprocal weight of the anatomical links and (b) matching index of input neighbours.

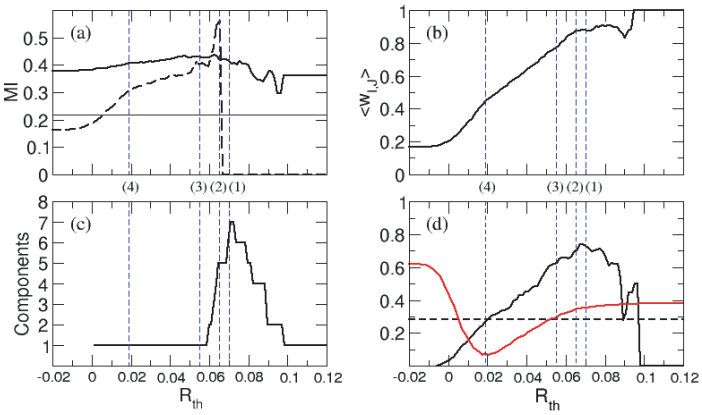

Figure 10. Properties of functional networks at various correlation thresholds. (a) Anatomical matching index of functional networks. Solid line, average of intracommunity links; dashed line, average MI of inter-community links; and horizontal line, global average of MI matrix (in figure 9(b)). (b) Average reciprocal weight of links expressed in M^{F}. (c) Number of connected components of M^{F}. (d) Hamming distance H (red line) between M^{A} and M^{F}, and modularity Q^{F} (black line) of M^{F} considering the four sub-divisions (V, A, SM, FL) versus R_{th}. Vertical lines correspond to the four snapshots in figure 11: (1) $R_{\mathrm{th}} = 0.070$, (2) $R_{\mathrm{th}} = 0.065$, (3) $R_{\mathrm{th}} = 0.055$ and (4) $R_{\mathrm{th}} = 0.019$.

which i and j connect (k stands for the degree of a node). With such a normalization $MI(I, J) = 1$ only if I and J receive input entirely from the same cortical areas, and $MI(I, J) = 0$ if all inputs to I and J come from completely different areas. The MI matrix from the anatomical connectivity is presented in figure 9(b). As can be seen, MI values of the areas within the anatomical communities V, A, SM and FL are high (internal MI). However, MI of areas in different communities (external) is heterogeneous, i.e. only some areas share many common neighbours with areas in other communities. To account for the functional implications of this anatomical feature, we average the MI of *functional connections*, provided areas belong to the same community (figure 10(a), bold line) or to different communities (dashed line).

Our goal is to study how much the pair-wise correlation between cortical areas depends on these two measures. Starting with a threshold R_{th} equal to the highest value in R_{IJ}, we proceed

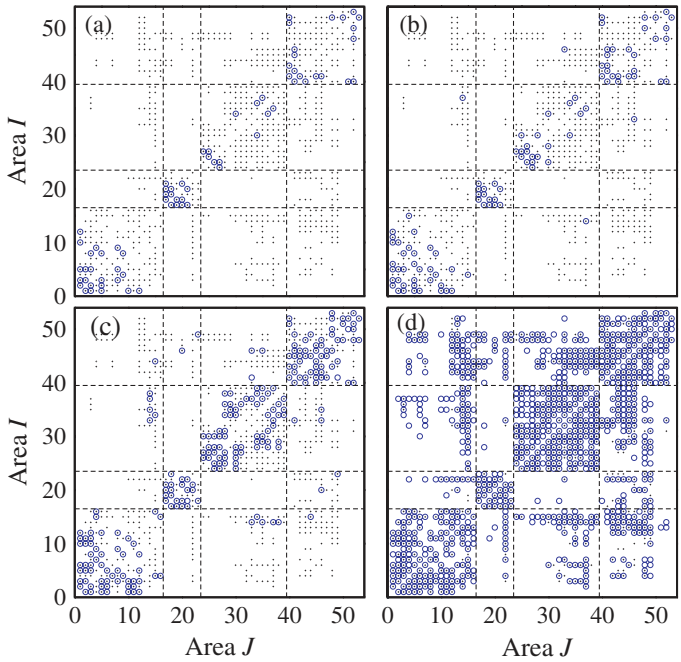

Figure 11. The functional networks (○) at various thresholds: $R_{\text{th}} = 0.070$ (a), $R_{\text{th}} = 0.065$ (b), $R_{\text{th}} = 0.055$ (c) and $R_{\text{th}} = 0.019$ (d). The small dots indicate the anatomical connections.

to extract functional networks M^{F} as R_{th} is lowered. For each M^{F}, considering *only* expressed areas and links, we calculate their average $\langle w_{IJ} \rangle$ and average $\langle MI \rangle$ values (figures 10(a) and (b)).

Additionally, due to sparseness of functional links at high R_{th} thresholds, functional networks are separated into several *connected components*, i.e. areas form groups that are internally connected but disconnected from each other. In figure 10(c) the number of connected components within each M^{F} is presented.

Now we proceed to discuss in detail the organization properties of functional networks at different levels of synchronization. Typical patterns of functional connectivity are shown in figure 11.

1. When R_{th} is very close to the maximal value of R, only few areas within the auditory system A are functionally connected, because of their strong anatomical links and sharing of many common neighbours. Note that in figure 10(b) $\langle w_{IJ} \rangle = 1$ for the highest thresholds meaning that these nodes are anatomically connected by strong bidirectional links. With lower values, e.g. $R_{\text{th}} = 0.07$ (figure 11(a)), about 2/3 of the areas are present but only 10% of the P2 links and none of the P1 links are present. This is manifested by high values of $\langle w_{IJ} \rangle$. Interestingly, all functional links correspond to anatomical connections within the communities V, A, SM, and FL, forming 'core' functional subnetworks. However, M^{F} is distributed into several components (figure 10(c)).
2. At lower values, e.g. $R_{\text{th}} = 0.065$ (figure 11(b)) the small components grow and merge. There are only five components closely following the anatomical communities. The small decrease of $\langle w_{IJ} \rangle$ shows that the new functional links correspond to strong and bidirectional anatomical connections. Internal $\langle MI \rangle$ remains high (figure 10(a), solid line), denoting that

anatomical communities are densely connected. Notice that the first inter-community functional links are also expressed. Precisely these links functionally connect the cortical areas that have many neighbours in common (although they belong to different communities). This is accounted for by the peak in the external $\langle MI \rangle$ (figure 10(a), dashed line).

3. Moving to slightly lower thresholds, e.g. $R_{\text{th}} = 0.055$ (figure 11(c)) a transition occurs in the organization of M^{F}. While more links are included within the anatomical communities, a few inter-community connections lead to the merging of all components into a big single one (figure 10(c)). This permits the communication between all cortical areas. At this stage only about $1/3$ of the anatomical P2 links and very few P1 links are expressed. With such low connection density M^{F} already resembles the main properties of M^{A}: high clustering and community structure. The anatomical connectivity is much denser. This suggests high robustness and the existence of many parallel paths of information processing.
4. With further decreasing of the threshold, e.g. at $R_{\text{th}} = 0.019$ (figure 11(d)), all P2 links are just fully expressed and about 70% of P1 links too. Meanwhile, about 4% of non-connected pairs (P0) establish significant functional connections (significance level ≈ 0.004), since they have many common neighbours. The functional network reveals rather faithfully the anatomical network (figure 11(d)).

Summarizing, we have observed that nodes connected by strong bidirectional links and possessing many common neighbours are highly correlated, and thus, they are the first ones to be expressed as functionally connected. The strongest correlation occurs between nodes within the same anatomical community. Besides, internal $\langle MI \rangle$ (figure 10(a), solid line) remains stable over all R_{th}, and is much higher than the global $\langle MI \rangle$ between all areas (figure 10(a), horizontal line). This confirms high functional similarity between areas within the same community (even though they are not necessarily anatomically connected) and illustrates the capability of different communities (V, A, SM and FL) to perform specialized information processing. Cortical areas belonging to different communities have, in general, few neighbours in common as seen in figure 9(b). This is also exposed by the fast decrease of external $\langle MI \rangle$ as the number of functional links increases with decreasing R_{th} (figure 10(a), dashed line). However, the peak at $R_{\text{th}} \sim 0.06-0.07$ shows that the expression of few inter-community functional links between certain cortical areas in different communities (with high functional similarity) triggers a transition where all areas merge into a single connected component. This potentially allows the integration of the specialized information.

To further compare the matrices M^{F} and M^{A} in a more quantitative manner, we take the binary matrix of M^{A} and symmetrize all P1 links and compute the Hamming distance H, i.e. the percentage of elements between M^{F} and the binary M^{A} that are different. The closeness is minimal between them at $R_{\text{th}} \approx 0.019$, with a very small Hamming distance $H = 0.074$ (figure 10(d), red line). It is interesting to note that this threshold is exactly where the full distribution of R starts to deviate from the Gaussian and the distribution of P2 links separates from that of the surrogate data (figure 8(a), vertical solid line). We find that such a natural choice of R_{th} always reproduces well the network topology with minimal H for all coupling strengths $0.04 \leqslant g \leqslant 0.08$.

The formation of communities can be quantified by modularity Q [26],

$$Q = \sum_k e_{kk} - a_k^2, \tag{8}$$

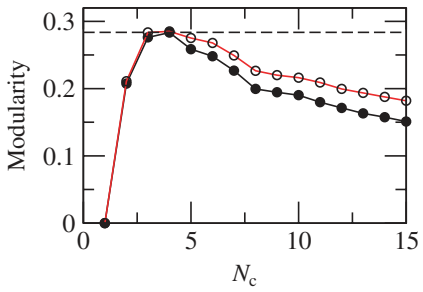

Figure 12. Modularities Q^C (○) and Q^A (●) versus the number of clusters N_c. The dashed line denotes Q^4.

with e_{kk} being the fraction of all links in the network that connect the nodes within community k, and $a_k = \sum_l e_{kl}$ is the fraction of edges from the whole network that connect to nodes in the community k. Figure 10(d), solid line, shows the modularity (Q^F) of the functional networks M^F at different thresholds considering the original anatomical communities V, A, SM and FL. For comparison, the modularity Q^4 calculated the four communities V, A, SM and FL, but with the anatomical connectivity M^A is shown: $Q^4 = 0.284$, horizontal dashed line in figure 10(d). In a broad range of R_{th}, Q^F is much larger than Q^4, and they coincide at the natural threshold $R_{th} = 0.019$ (figure 10(d)). This provides meaningful insights into how densely connected cortical subsystems (e.g. communities V, A, SM, FL) can perform highly specialized functions (the strongest synchronization) by a subset of areas and connections.

The above analysis based on functional networks suggests that the dynamics of the network is hierarchically clustered and that the most prominent clusters are consistent with the four known anatomical communities. A typical hierarchical tree in the weak coupling regime is shown in figure 10(a). At each level of the tree, a set of N_c clusters is detected (see section 4.4). What are the underlying topological links within and across these dynamical clusters? We calculate both the anatomical modularity Q^A (using the anatomical matrix M^A) and the functional modularity Q^C (using the correlation matrix R_{IJ}). The difference of Q^C and Q^A from Q^F and Q^4 (figure 10(c)) is that Q^F and Q^4 are obtained for the 4 cortical subsystems V, A, SM, FL using M^F and M^A. respectively. Now, we define Q^C as an extension of Q in equation (8) to use the values of the correlation matrix (without threshold) instead of the connectivity matrix:

$$e_{kl} = \sum_{I \neq J} R_{IJ}, \quad \text{where } I \in k,\ J \in l. \quad k, l = 1, \ldots, N_c. \tag{9}$$

So e_{kl} is the fraction of the total strength of correlation between communities k and l. Strikingly, at different levels of the hierarchy (varying N_c), Q^C and Q^A follow each other closely (figure 12). This provides strong evidence that the dynamical organization reveals hierarchical scales in the network topology. At $N_c = 4$, both Q^C and Q^A are maximal, approaching Q^4 of the four communities in the anatomical network. Thus the dynamical clusters agree well with the anatomical communities.

4.4. Transition of cluster formation

We have analysed the most prominent dynamical clusters using an algorithm for hierarchical clustering in Matlab with the dissimilarity matrix $d = [d(I, J) = 1 - R_{IJ}]$. Typical hierarchical trees (dendrograms) for three different synchronization regimes are shown in figure 13.

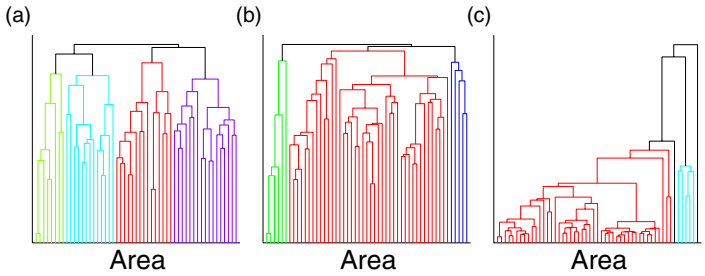

Figure 13. Typical hierarchical tree of the dynamical clusters in the weak coupling regime (a) $g = 0.07$, transient regime (b) $g = 0.082$ and strong coupling regime (c) $g = 0.12$.

In dendrograms the height of each line connecting two objects (areas or clusters) represents their distance. The higher the lines, the more distant the objects are, and so they are less likely to belong to the same group. At weak coupling, the nodes preserve their own dynamics, correlation is low and thus the distance between individual areas is relatively high. Looking at the highest levels of the hierarchical tree, one can see how the brain areas form the four main dynamical clusters (figure 13(a)). By increasing the coupling strength, the areas exhibit higher correlation of the activity, leading to the formation of one dominant and two small additional clusters (figure 13(b)). In the next step, due to the strong coupling, the mean activity of the majority of areas is strongly synchronized; this is also expressed by the short distance between the individual objects. Most of the areas merge into two major clusters, but a few areas still preserve their own dynamics (figure 13(c)). Here the distance between the clusters is large, because of different dynamics. The details of the major clusters in all these three cases of coupling strength are presented in figures 14–16.

Figure 14 displays the most prominent functional clusters for the weak coupling regime. They follow closely the four anatomical communities – C_1 (V), C_2 (A), C_3 (SM), C_4 (FL). However, there are a few nodes which belong to one anatomical community but join another dynamical cluster. For example, the area $I = 49$ (anatomically named 'area 36') of the fronto-limbic system appears in the dynamical cluster C_2 mainly composed of areas from the auditory system (figure 14(C_2)). A closer inspection shows that these nodes bridging different anatomical communities and dynamical clusters are exactly the areas sitting in one anatomical community but in close connectional association with the areas in other communities [4]. More detailed analysis of these bridging areas can be found in [20].

The transient regime between the weak and strong couplings is characterized by the formation of one major cluster and two small clusters (figure 15). This major cluster C_1 consists of the somato-motor system and absorbs most of the visual areas and about half of the FL system and one area from the auditory system (figure 15(C_1)). The cluster C_2 corresponding to the auditory system A remains relatively independent, connected only through area 22 to the central cluster C_1 (figure 15(C_2)).

In the strong synchronization regime, V, SM and FL join to form a major cluster (figure 16(C_1)). The auditory system A is still independent (figure 16(C_2)). The formation of an independent cluster from the community A both in the weak and the strong synchronization regimes is due to almost global connections within A and few intercommunity connections to others. The cluster formation behaviour in the strong coupling regime is also in good accordance

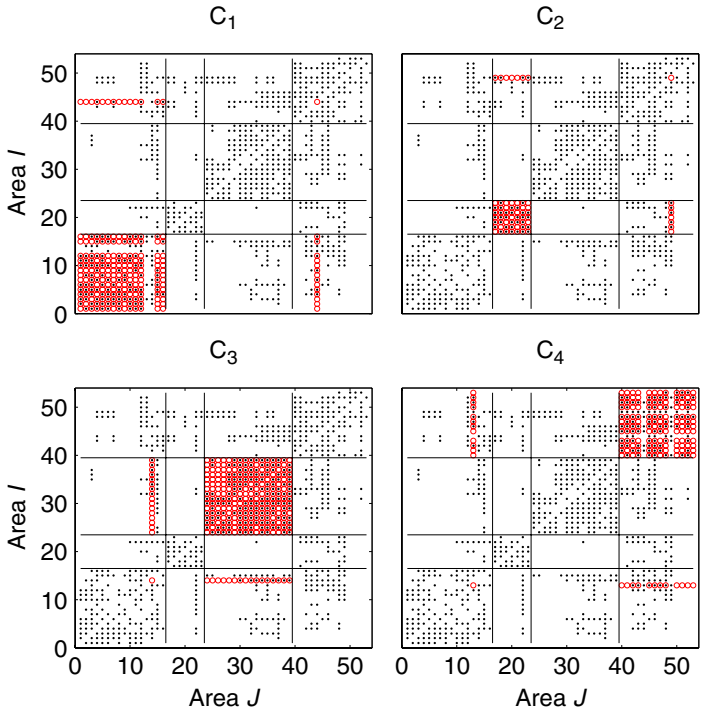

Figure 14. Four major dynamical clusters (○) with weak coupling strength $g = 0.07$, compared to the underlying anatomical connections (·).

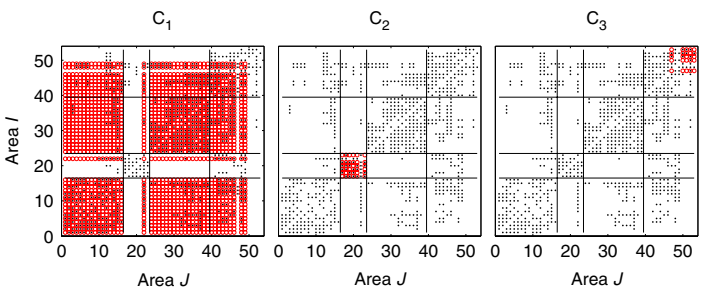

Figure 15. Three major dynamical clusters (○) with intermediated coupling strength $g = 0.82$, compared to the underlying anatomical connections (·).

with the inter-community connectivity shown in figure 1(b). There are also two single areas showing rather independent dynamics. It turns out that these are the nodes with the minimal intensities in the network ($S_{53} = 8$ and $S_8 = 11$). In [20] we have shown that the clustering patterns remain almost the same in randomized networks that preserve the sequence of the intensities S_I as in the cat cortical network; the auditory system A no longer forms a distinct cluster when the pronounced intra-community connections are destroyed by randomization. This demonstrates that our understanding of synchronization based on mean field approximation in section 3 can be applied when the node dynamics (mean activity of the subnetwork in this case) displays a well-defined oscillatory behaviour.

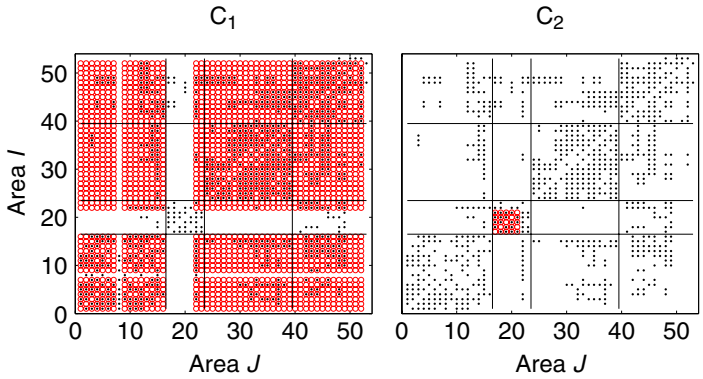

Figure 16. Two major dynamical clusters (○) with strong coupling strength $g = 0.12$, compared to the underlying anatomical connections (·).

The comparison between the multilevel model and the population model indicates that self-sustained oscillator models may not be as appropriate for the understanding of the interplay between dynamics and structure in the brain as a *hierarchical network of excitable elements*.

5. Conclusion and outlook

We have studied synchronization in a realistic network of cat cortical connectivity. We have demonstrated that if well-defined oscillatory dynamics are assumed for the nodes (cortical areas composed of large ensembles of neurons), the synchronization patterns are mainly controlled by the global structural statistics of the nodes (input intensities). This happens, for example, by representing the areas through a neural mass model, or by a subnetwork of rather strongly coupled neurons. However, a multilevel model with weak coupling displays biologically plausible dynamics, and the synchronization patterns exhibit a close relationship to the hierarchically clustered organization of the anatomical topology. The dynamics are mainly controlled by the detailed organization of the network connectivity, such as the reciprocity of the directed connections and the common environment of a pair of areas. The activity of the subnetwork in the weak coupling regime displays a broad frequency spectrum, however, it does not reproduce pronounced rhythmic oscillations as observed in EEG of real brain activity. An improved model capturing both properties would bring a deeper understanding of the structure–function relation, which is reasonably speculated to lie between the above two cases.

Here we have only focused on the highest structural level and modelled each large cortical area with one sublevel of neurons with simple dynamics. In a biologically plausible regime (weak coupling regime), the maximal correlation values are low $(0.1-0.2)$. In the strong coupling regime the dynamics display a large region of frequent and regular spiking of the neurons and strong synchronization even without external influence. The maximum correlation values for actual functional connectivity can be considerably higher [9]. The strong correlation between spatially close brain regions obtained from high spatial resolution fMRI data is mainly due to dense connectivity within local neuronal ensembles [9], while the relatively strong correlation between distant functional areas, especially in the low frequency bands, may have a close relation to the underlying long-range projections [11]. The difference between our model and

experimental observation could be mainly due to the one-level connectivity in the subnetwork, which does not allow strong activation within a subnetwork without propagating to excite the whole network.

Although still rather simplified, the present multilevel model already displays plausible clustering dynamics, and the most prominent clusters are consistent with the underlying network communities and the functional subdivision of the cortical systems.While prediction at the level of individual connections may not be justified from the model at this stage, the results at the level of prominent clusters are already quite suggestive. It is meaningful to examine the relationship between the functional clusters and the functional subdivisions of the human cortex from data. The information for both is available: the functional clusters can be obtained from brain imaging data and the organization of functional areas into sub-cortical systems (visual, auditory etc) is already known [11].

The model can be extended and improved in several ways, in order to capture more realistic information processing in the brain. (i) Biologically, a system in the order of 10^5 neurons, corresponding to a cubic millimetre of cortex, is the minimal system size at which the complexity of the cortex can be represented (where the number of synapses a neuron receives is around 10^4) [40, 41]. Thus, large subnetworks with other biologically realistic features, e.g. organization of neurons into layers and columns, and more detailed spatial structure of neural circuits should be considered. Such an extension is important for the modelling and simulation of experimentally observed hierarchical activity characterized by synchronization phenomena over a wide range of spatial and temporal scales. (ii) Cortical and subcortical neurons exhibit rich dynamics [42], for example, tonic spiking and burst firing modes which are related to wakefulness and sleep [43]. These different firing modes have significant effects on the synchronization of coupled neurons [44], which may affect global functional connectivity. More subtle neural models are required to account for richer neuronal dynamics. (iii) Biologically more realistic coupling by chemical synapses should be used and synaptic plasticity considered.

These more realistic implementations might allow significant improvement in the modelling of EEG by generating both rhythmic oscillations and a broad-band background activity. The hierarchical network architectures would also allow localized and strong synchronization in some low-level clusters and naturally organized dynamics at higher levels. The biologically plausible regimes may be significantly broaden, with stronger correlations similar to that observed experimentally [11].

In future the proposed framework will be used to investigate the relative contributions of network topology and task-related network activations to specific functional brain connectivity and information processing. The study is very relevant to the analysis of the event-related brain potential (ERP) in cognitive studies. Classical ERP analysis assumes that the stimulus-evoked response is independent of the on-going spontaneous activity, so that EEG measurements can be averaged over many trials to look for the offset to the reference state [45]. However, the on-going spontaneous activity between different brain areas in a no-task state is not independent, but displays sophisticated connectivity [8]–[11]. Here we demonstrated with the multilevel model that the functional connectivity is governed by the underlying complex network topology. Since both the stimulus-evoked response and the background activity occur on the same underlying neuronal network, such an assumption of independence between them is challenged. In fact, simulations of neurons on a simple array demonstrate that the response of the system to external stimuli can be significantly modified, especially enhanced in the presence of background activity and coupling [46]. This suggests that there exist nontrivial, nonlinear interactions between the

stimulus-evoked response and the on-going background activity, and the interplay could be much more complicated in hierarchical network architectures and may have significant contributions to the ERP components. Thus, the analysis of ERP generation with the model proposed here can aid our understanding of the neurobiological foundation of cognition and provide guidance for improved ERP analysis in cognitive studies.

Furthermore, the model dynamics could be compared to the observed activity spread in the cortex [47] and to the functional connectivity [9]–[11] at suitable spatio-temporal scales. With recently developed approaches for dynamic causal modelling of evoked responses in the brain using functional imaging and coupled neural mass models, the effective functional connectivity at the highest scale, i.e. between functional areas involved in the processing, can be explored [31]. The multilevel, hierarchical cluster model proposed here would allow the investigation of the structure–function relationship over a range of scales. This should shed light on understanding how the hierarchical synchronization dynamics [2] is raised from the underlying hierarchy of structural connectivity [3] in the brain. This achievement would require further developments in neurophysics, in the theory of dynamical complex networks, in algorithms of parallel computing [41] as well as in experimental approaches for high-resolution functional recordings.

Acknowledgments

We thank A Arenas and R Steuer for interesting discussions. This work was supported by Helmholtz Institute for Mind and Brain Dynamics, Helmholtz Institute for Supercomputational Physics and EU-Network BioSim, contract no. LSHB–CT–2004–005137.

References

[1] Salinas E and Sejnowski T J 2001 *Nat. Rev. Neurosci.* **2** 539–50
Fries P 2005 *Trends Cogn. Sci.* **9** 474–80
Schnitzler A and Gross J 2005 *Nat. Rev. Neurosci.* **6** 285–96
[2] Stam C J and de Bruin E A 2004 *Hum. Brain Mapp.* **22** 97–109
Breakspear M and Stam C J 2005 *Phil. Trans. R. Soc.* B **360** 1051–74
[3] Sporns O, Tononi G and Kötter R 2005 *PLoS Comput. Biol.* **1** 0245–51
[4] Scannell J W, Burns G A P C, Hilgetag C C, O'Neill M A and Young M P 1999 *Cereb. Cortex* **9** 277–99
[5] Felleman D J and van Essen D C 1991 *Cereb. Cortex* **1** 1–47
[6] Sporns O, Chialvo D R, Kaiser M and Hilgetag C C 2004 *Trends Cogn. Sci.* **8** 418–25
[7] Kaiser M, Martin R, Andras P and Young M P 2007 *Eur. J. Neurosci.* at press
[8] Bassett D S and Bullmore E 2006 *Neuroscientist* **12** 512–23
[9] Eguíluz V M, Chialvo D R, Cecchi G, Baliki M and Apkarian A V 2005 *Phys. Rev. Lett.* **94** 018102
[10] Stam C J 2004 *Neurosci. Lett.* **355** 25–8
[11] Salvador R *et al* 2005 *Cereb. Cortex* **15** 1332–42
Achard S, Salvador R, Whitcher B, Suckling J and Bullmore E 2006 *J. Neurosci.* **26** 63–72
Bassett D S, Meyer-Lindenberg A, Achard S, Duke T and Bullmore E 2006 *Proc. Natl Acad. Sci. USA* **103** 19518–23
[12] van Vreeswijk C and Somoplinsky 1996 *Science* **274** 1724–6
van Vreeswijk C and Somoplinsky 1998 *Neural Comput.* **10** 1321–71
Brunel N 2000 *J. Comput. Neurosci.* **8** 183–208
[13] Kudela P, Franaszczuk P J and Bergey G K 2003 *Biol. Cybern.* **88** 276–85
[14] Binzegger T, Douglas R J and Martin K A C 2004 *J. Neurosci.* **24** 8441–53

Schubert D, Kötter R, Luhmann H J and Staiger J F 2006 *Cereb. Cortex* **16** 223–36
Markram H, Toledo-Rodriguez M, Wang Y, Gupta A, Silberberg G and Wu C 2004 *Nat. Rev. Neurosci.* **5** 793–807
[15] Markram H 2006 *Nat. Rev. Neurosci.* **7** 153–60
[16] Lopes da Silva F H, Hoeks A, Smits H and Zetterberg L H 1974 *Kybernetik* **15** 27–37
[17] Wendling F, Bellanger J J, Bartolomei F and Chauvel P 2000 *Biol. Cybern.* **83** 367–78
[18] Buzsaki G, Geisler C, Henze D A and Wang X J 2004 *Trends Neurosci.* **27** 186–93
[19] Zemanová L, Zhou C S and Kurths J 2006 *Physica* D **224** 202–12
[20] Zhou C S, Zemanová L, Zamora G, Hilgetag C C and Kurths J 2006 *Phys. Rev. Lett.* **97** 238103
[21] Sporns O and Zwi J D 2004 *Neuroinformatics* **2** 145–62
[22] Hilgetag C C and Kaiser M 2004 *Neuroinformatics* **2** 353–60
[23] Zamora G, Zhou C S and Kurths J 2007 *Lectures on Supercomputational Neuroscience*: *Complex Networks in Brain Dynamics, Springer Series of Understanding Complex systems* (Berlin: Springer) at press
[24] Hilgetag C C, Burns G A P C, O'Neill M A, Scannell J W and Young M P 2000 *Phil. Trans. R. Soc. Lond.* B **355** 91–110
[25] Newman M E J and Girvan M 2004 *Phys. Rev.* E **69** 026113
Newman M E J 2004 *Eur. Phys. J.* B **38** 321–30
Arenas A, Díaz-Guilera A and Pérez-Vicente C J 2006 *Phys. Rev. Lett.* **96** 114102
[26] Niedermeyer E and Lopes da Silva F H 1993 *Electroencephalography: Basic Principles, Clinical Applications, and Related Fields* (Baltimore: Williams and Wilkins)
Kandel E R, Schwartz J H and Jessell T M 2000 *Principles of Neural Science*, 4th edn (New York: McGraw-Hill)
[27] David O and Friston K J 2003 *NeuroImage* **20** 1743–55
[28] Motter A E, Zhou C S and Kurths J 2005 *Phys. Rev.* E **71** 016116
Zhou C S, Motter A E and Kurths J 2006 *Phys. Rev. Lett.* **96** 034101
Zhou C S and Kurths J 2006 *Phys. Rev. Lett.* **96** 164102
[29] Milo R, Shen-Orr S, Itzkovitz S, Kashtan N, Chlkovskii D and Alon U 2002 *Science* **298** 824–7
[30] David O, Harrison L and Friston K J 2005 *NeuroImage* **25** 756–70
[31] David O, Kiebel S, Harrison L, Mattout J, Kilner J M and Friston K J 2006 *NeuroImage* **30** 1255–72
[32] Watts D J and Strogatz S H 1998 *Nature* **393** 440–2
[33] Lago-Fernández L F, Huerta R, Corbacho F and Sigüenza J A 2000 *Phys. Rev. Lett.* **84** 2758–61
[34] Masuda N and Aihara K 2004 *Biol. Cybern.* **90** 302–9
[35] Guardiola X, Díaz-Guilera A, Llas M and Pérez C J 2000 *Phys. Rev.* E **62** 5565–70
[36] Roxin A, Riecke H and Solla S A 2004 *Phys. Rev. Lett.* **92** 198101
[37] Young M P 2000 *Spatial Vis.* **13** 137–46
[38] FitzHugh R 1961 *Biophys. J.* **1** 445–66
Pikovsky A S and Kurths J 1997 *Phys. Rev. Lett.* **78** 775–8
[39] Hilgetag C C, Kötter R, Stephan K E and Sporns O 2002 *Computational Neuroanatomy* (Totowa, NJ: Humana Press) 295–336
[40] Braitenberg V and Schüz A S 1991 *Anatomy of the Cortex: Statistics and Geometry* (Berlin: Springer)
[41] Morrison A, Mehring C, Geisel T, Aertsen A and Diesmann M 2005 *Neural Comput.* **17** 1776–801
[42] Izhikevich E M 2004 *IEEE Trans. Neural Netw.* **15** 1063–70
[43] McCormick D A and Feeser H R 1990 *Neuroscience* **39** 103–13
Saper C B, Scammell T E and Lu J 2005 *Nature* **43** 1257–63
[44] Postnova S, Wollweber B, Voigt K and Braun H 2007 *Biosystems* **89** 135–42
[45] Hohlfeld A and Sommer W 2005 *Cogn. Brain Res.* **24** 500–12
Martin-Loeches M, Nigbur R, Casado P, Hohlfeld A and Sommer W 2006 *Brain Res.* **1093** 178–89
[46] Zhou C S, Kurths J and Hu B 2003 *Phys. Rev.* E **67** 030101R
[47] Kötter R and Sommer F T 2000 *Phil. Trans. R. Soc. Lond.* B **355** 127–34